Electromagnetic wave absorbing properties of aligned amorphous carbon nanotube/BaFe12O19 nanorod composite

Zhao, Tingkai; Ji, Xianglin; Jin, Wenbo; Guo, Shasha; Zhao, Haoyu; Yang, Wenhui; Wang, Zinqui; Xiong, Chuanyin; Dang, Alei; Li, Hao; Li, Teihu; Shang, Songmin; Zhou, Zhongfu

Published in:
Journal of Alloys and Compounds

DOI:
10.1016/j.jallcom.2017.02.014

Publication date:
2017

Citation for published version (APA):
Zhao, T., Ji, X., Jin, W., Guo, S., Zhao, H., Yang, W., Wang, Z., Xiong, C., Dang, A., Li, H., Li, T., Shang, S., & Zhou, Z. (2017). Electromagnetic wave absorbing properties of aligned amorphous carbon nanotube/BaFe12O19 nanorod composite. *Journal of Alloys and Compounds*, *703*, 424-430. https://doi.org/10.1016/j.jallcom.2017.02.014

Accepted Manuscript

Electromagnetic wave absorbing properties of aligned amorphous carbon nanotube/ $BaFe_{12}O_{19}$ nanorod composite

Tingkai Zhao, Xianglin Ji, Wenbo Jin, Shasha Guo, Haoyu Zhao, Wenhui Yang, Xinqi Wang, Chuanyin Xiong, Alei Dang, Hao Li, Tiehu Li, Songmin Shang, Zhongfu Zhou

PII: S0925-8388(17)30430-9

DOI: 10.1016/j.jallcom.2017.02.014

Reference: JALCOM 40742

To appear in: *Journal of Alloys and Compounds*

Received Date: 19 November 2016

Revised Date: 30 January 2017

Accepted Date: 3 February 2017

Please cite this article as: T. Zhao, X. Ji, W. Jin, S. Guo, H. Zhao, W. Yang, X. Wang, C. Xiong, A. Dang, H. Li, T. Li, S. Shang, Z. Zhou, Electromagnetic wave absorbing properties of aligned amorphous carbon nanotube/$BaFe_{12}O_{19}$ nanorod composite, *Journal of Alloys and Compounds* (2017), doi: 10.1016/j.jallcom.2017.02.014.

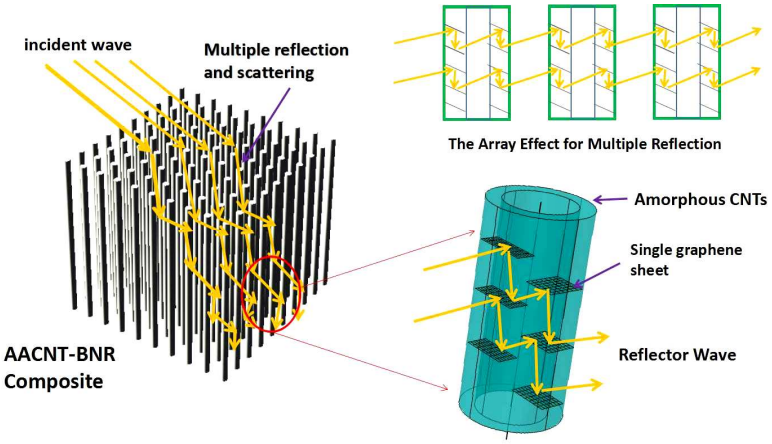

Electromagnetic wave absorbing properties of aligned amorphous carbon nanotube/$BaFe_{12}O_{19}$ nanorod composite

Tingkai Zhao[1,*], Xianglin Ji[1,*], Wenbo Jin[1], Shasha Guo[1], Haoyu Zhao[1], Wenhui Yang[1], Xinqi Wang[1], Chuanyin Xiong[1], Alei Dang[1], Hao Li[1], Tiehu Li[1], Songmin Shang[2], Zhongfu Zhou[3]

[1] *State Key Laboratory of Solidification Processing, Shaanxi Engineering Laboratory for Graphene New Carbon Materials and Applications, School of Materials Science and Engineering, Northwestern Polytechnical University, Xi'an 710072, China*

[2] *Institute of Textiles and Clothing, The Hong Kong Polytechnic University, Kowloon, Hong Kong*

[3] *Department of Physics, Aberystwyth University, Aberystwyth SY23 3FL, UK*

Abstract: Aligned amorphous carbon nanotube (AACNT)/$BaFe_{12}O_{19}$ nanorod (BNR) composite was prepared by chemical vapor deposition and ball-milling methods. Raman and XRD tests were performed to investigate the microstructures, and the microwave absorbing properties of the as prepared composite were characterized using a vector network analyzer. The experimental results indicated that the mean length of as-prepared ACNT arrays was about 24 μm and the average length of BNRs were about 50 nm. The maximum absorbing peak of AACNTs/BNR composite is -21.5 dB at the frequency of 9.3 GHz. The frequency bandwidth of the reflectivity loss below -10 dB is about 2.5 GHz. AACNTs have both features of amorphous CNTs which have multiple-reflective path inside the tube-wall and crystalline CNTs which

[*] Corresponding author. E-mail address: ztk-xjtu@163.com (T.K. Zhao) and jixianglinnwpu@163.com (X.L. Ji)

T.K. Zhao and X.L Ji contribute equally to this work.

have high conductivity.

Keywords: Amorphous carbon nanotubes (ACNTs); Aligned array; $BaFe_{12}O_{19}$ nanorods (BNRs); Electromagnetic wave absorbing properties

1. Introduction

Since the discovery of carbon nanotubes (CNTs) **[1]** by Iijima, CNTs have attracted tremendous attention due to their unique structures, high thermal conductivity, excellent electrical and electronic properties, extraordinary mechanical strength, and unique magnetic and optical performance. Up to the present, diverse range of potential applications **[2-7]** such as hydrogen storage, lithium batteries, sensors and probes are related to CNTs. There are mainly three synthesis methods for CNTs, namely laser ablation (LA), arc discharge (AD), and chemical vapor deposition (CVD). For the synthesis of crystalline CNTs, the requirement of expensive production costs, complex processing steps, long synthesis period, catalyst support and high operating temperature are inevitable. However, the synthesis requirements of amorphous CNTs (ACNTs) are gentle, with lower growth temperature and simple procedures. At present, ACNTs **[8,9]** draw more and more attention due to its defective amorphous tube-wall structures, and simple synthesis methods, large quantities and low costs **[10]**.

Recently, electromagnetic wave absorption materials with favorable properties such as low density, low cost, strong absorption and thin thickness within a wide frequency range are strongly needed due to the rapid development of electronic

devices, electromagnetic wave communication and the pollution of electromagnetic interference **[11,12]**. For the relative complex permittivity to both real (dielectric constant) and imaginary (magnetic loss) components, the parameter requirements for electromagnetic wave absorption are well established. The performance of electromagnetic wave absorption is dominated by the complex permittivity and the microstructure of absorber material. The materials used as electromagnetic wave absorbers must have higher energy loss with high imaginary component of permittivity and enable better absorption of incident radiation in synchronized frequencies by dissipating it as heat. Generally, according to the magnetic and dielectric loss characteristics, there are two kinds of electromagnetic wave absorber materials, namely magnetic loss and dielectric absorbers. For the absorption at electromagnetic wave frequency, $BaFe_{12}O_{19}$ powder **[13-15]** is known to be ideal fillers for developing electromagnetic absorber materials due to its high stability, low density, low cost, large electrical resistivity and high magnetic loss. However, their applications are limited by poor dielectric constant. Nowadays, the absorber composites consisting of both dielectric and magnetic fillers have much attention. Especially, CNTs **[16-18]** could fulfill those requirements due to their light weight, good conductivity, physical and chemical stability. There has been strong interest to develop hybrid materials **[19-21]** both $BaFe_{12}O_{19}$ nanostructures and CNTs for further characterization. This new type of absorber composite is highly demanded to develop new electromagnetic wave absorption materials. CNTs as conductive filler have been widely used as absorber materials and they have strong electromagnetic wave

absorbing properties within GHz frequency range. Compared with CNTs, ACNTs, due to its defective amorphous tube-wall structures, and simple synthesis methods, large quantities and low costs, will have more excellent electromagnetic wave absorbing performance than CNTs **[10]**. However, although the good microwave absorbing properties of ACNTs, there are not many researches focusing on the further discussion about the ACNT/$BaFe_{12}O_{19}$ hybrid material, especially the ACNTs array, which will further improve the electromagnetic properties due to the multiple reflection.

In this work, aligned ACNT (AACNT)/$BaFe_{12}O_{19}$ nanorod (BNR) composite was prepared through CVD and ball-milling methods. For comparison, CNTs, ACNTs and AACNTs were synthesized to investigate the influences of the amorphous structure as well as the array structure on the electromagnetic wave absorbing performance. Possible assumptions were proposed to explain the electromagnetic properties of these three CNT structures.

2. Experimental

The synthesis process of AACNTs-BNR composite mainly contains three steps (see Fig.1). Firstly, AACNTs were fabricated using floating catalyst method. The xylene was used as carbon source and ferrocene and silane were used as catalyst precursor. Secondly, BNRs were synthesized by self-propagating combustion using citric acid complex $Fe(NO_3)_3$, $Ba(NO_3)_3$ as precursor. Then, the obtained AACNTs were purified using dilute hydrochloric acid and then mixed with BNRs using ball-milling machine followed by 800□ heating for two hours. Finally, the AACNT/BNR composite was fabricated.

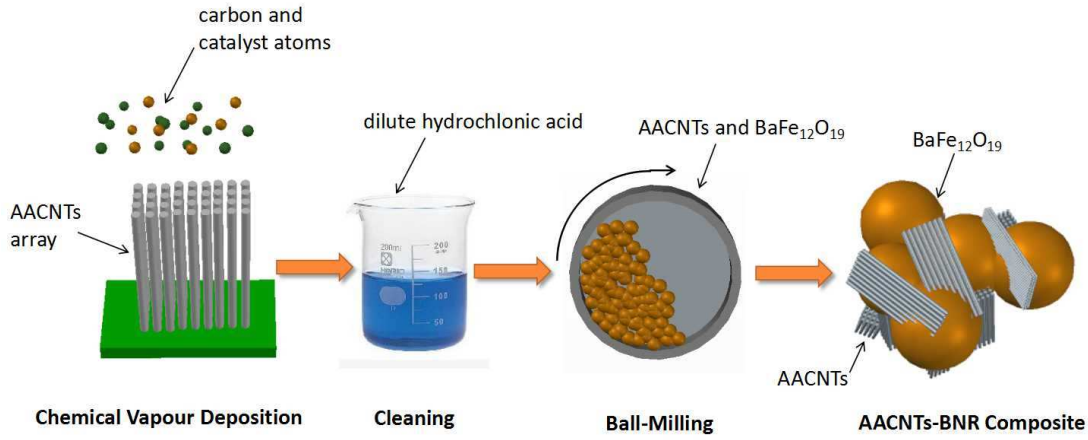

Fig. 1 The fabrication process schematics of AACNT/BNR composite

2.1 Synthesis of ACNT array

The growth of AACNTs was similar with our previous work **[4]**, performed by floating catalyst CVD in a quartz tube reactor (length 80 cm and diameter 5 cm). The reaction temperature was set at 770 □, and argon gas controlling the flow speed of 200 sccm was used as the carrier gas. The xylene (analytical pure grade), ferrocene (analytical pure grade) and triethylsilane (analytical pure grade) solution (the mole ratio of C: Fe: Si is 30: 1: 0.1) were used as carbon source and catalyst precursor which was injected into the reactor by a syringe pump at the speed of 0.3 ml/min. The samples were obtained from the surface of the tube reactor and collected for further characterization.

2.2 Synthesis of $BaFe_{12}O_{19}$ nanorods

The BNRs were synthesized by self-propagating combustion using citric acid complex $Fe(NO_3)_3$, $Ba(NO_3)_3$ as precursor and the mass ratio of $Fe(NO_3)_3$ (analytical pure grade), $Ba(NO_3)_3$ (analytical pure grade) and citric acid (analytical pure grade) is 11:1:13. The ingredients were firstly dissolved into distilled water and then ammonium hydroxide was added to adjust pH to 7. The obtained colloidal sol was

dried at 120 □. The dried gel was heated at 400 □ for giving rise to the self-propagating combustion. After the reaction, the powders were collected and then cleaned by distilled water to get rid of the residual ingredients for further application.

2.3 Synthesis of AACNT/BNR composite

The as prepared AACNTs, ACNTs [22] and purchased CNTs (purity: >95%, average diameter: 20 nm, Tsinghua University, China) were cleaned in dilute hydrochloric acid to get rid of impurities. Then the AACNTs, ACNTs and CNTs were mixed with $BaFe_{12}O_{19}$ using ball-milling machine. Finally, the resulting samples were transferred into the tube furnace to heat processing at 800 □ for 2 hrs under Ar gas protection.

2.4 Characterizations

Transmission electron microscope (TEM, Tecnai G2 F30, FEI), field emission scanning electron microscope (FE-SEM, JSM-6700F, JEOL), X-ray diffraction patterns with Cu K_a radiation (XRD, X'Pert PRO MPD, PANalystal, λ=0.154 nm) and the Raman scattering spectrum (514 nm, LabRAM HR800, HORIBA JOBIN YVON) are used for qualitative analyses on the surface morphology, structural properties and component composition of all samples. The samples which were used for the characterization of electromagnetic wave absorbing properties were prepared by mixing 70 wt.% AACNT/BNR composite with 30 wt.% molten paraffin, then made into a rectangular waveguide (22.86 mm in length, 10.16 mm in width and 2 mm in thickness). The complex permittivity (ε', ε'') and permeability (μ', μ'') components as the function of frequency of a sample are measured using MS4644A Vector-network

Analyzer (VNA, Anritsu: 10 MHz–40 GHz).

3. Results and discussion

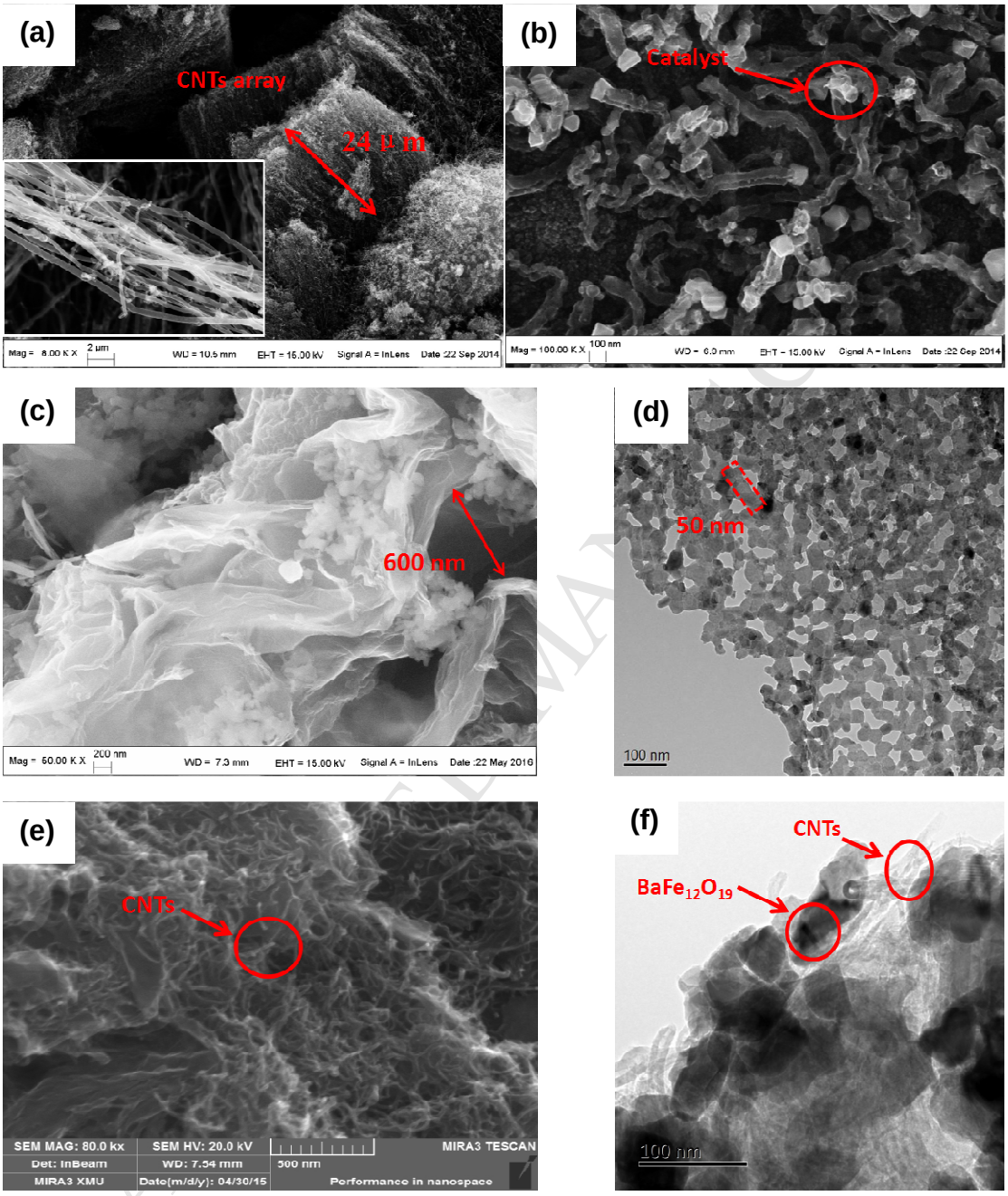

Fig. 2 Microstructures of AACNTs, BNR and AACNT/BNR samples, Fig. 2a is SEM image of AACNT array; Fig. 2b is SEM image of AACNT tip-end; Fig. 2c is SEM image of BNRs; Fig. 2d is TEM image of BNRs. Fig. 2e is SEM image of AACNTs incorporated with $BaFe_{12}O_{19}$; Fig. 2f is TEM image of AACNT/BNR composite

Fig. 2a is SEM image of AACNTs sample scratched from the quartz tube. It can be seen that after 30 min growth, the mean length of the CNT array reaches at around 24 μm. The formation of the array is due to the high density of the CNTs, because there is not enough space for CNTs to grow into other directions but squeeze each other into vertical direction. It can be seen from the enlarged picture inside Fig. 2a that CNTs are grown into the same direction and formed into a bunch because of the Van der Waals force. There are lots of impurities among AACNT soot, which might be due to the high injection rate and large quantities of carbon source. According to this phenomenon, it can be assumed that the higher concentration of carbon atoms in the reactive process might be one of the reasons that can promote the formation of amorphous tube-wall structure, while the decomposition rate of carbon source is far higher than that of the catalyst precursor leading to the excess of carbon atoms. There might be not enough time for large amounts of carbon clusters to form carbon crystal lattice structures on the surface of the catalyst particles, and it leads to the formation of amorphous structures. Besides, the other possible reason mentioned in our previous work **[4]** is that the adding of Si elements in the catalyst might distort the ordered crystal structure of Fe particles by forming alloy compound and then leads to the unstable and irregular precipitation of carbon atoms, which also causes the formation of amorphous structures. Fig. 2b is SEM image of AACNT tip-end. There exist metal particles with different shapes on the top of tube-mouth, which may prove the top-down growth mechanism in this process. The mean diameter of CNTs is similar with that of the particles around 70 nm. It can be concluded that the diameter of CNTs

might be controlled through the adjustment of catalyst concentration. Fig. 2c is SEM image of BNRs. It can be seen that BNRs appear to like multi-pore flowers having a layer by layer structure. The pores diameter inside the sample is about 600 nm indicating a low density. Fig. 2d is TEM image of BNRs. The average length of the rods is about 50 nm and the nanorods aggregate together forming the porous structures and low density structure of $BaFe_{12}O_{19}$, which further expands the application in electromagnetic wave absorbing field. Fig. 2e and Fig. 2f is SEM and TEM image of AACNT/BNR composite respectively. The CNTs are incorporated inside the $BaFe_{12}O_{19}$ nanopores. AACNTs and the $BaFe_{12}O_{19}$ are well connected with each other in the nanostructures.

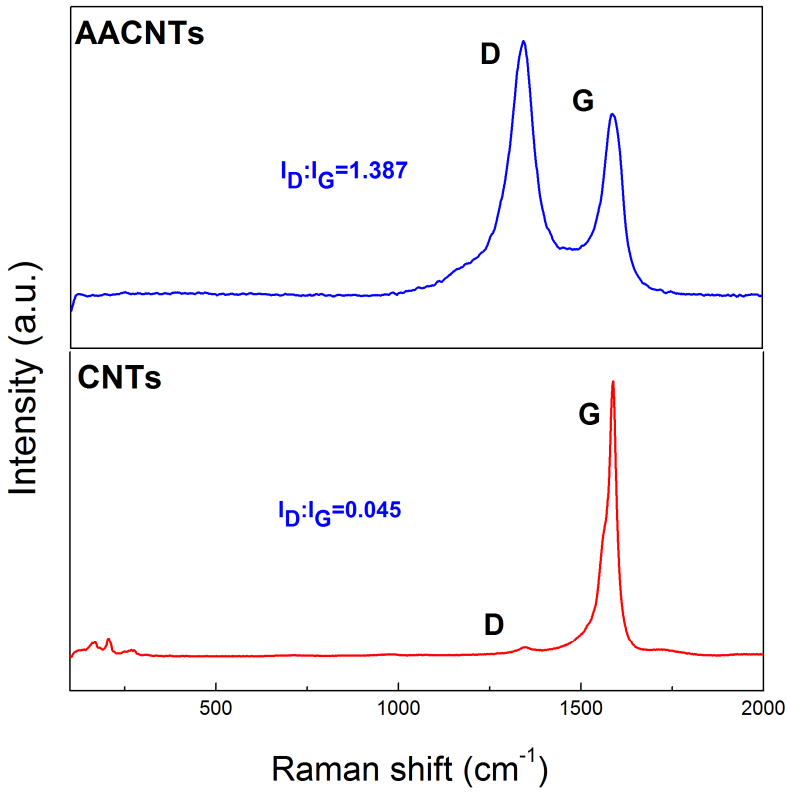

Fig. 3 Raman spectra of AACNTs

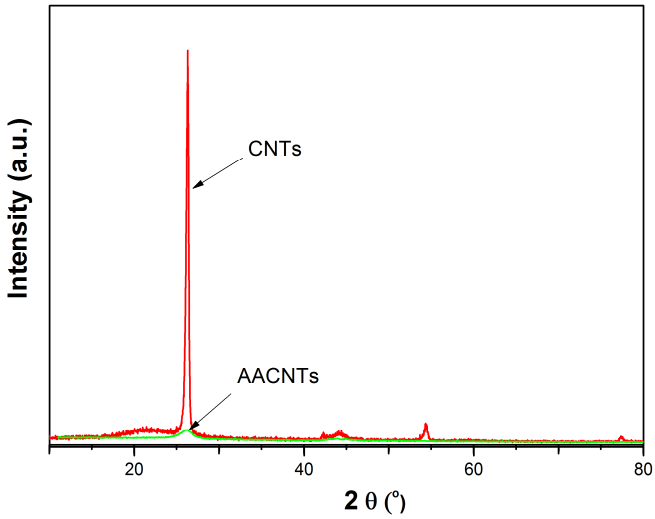

Fig. 4 XRD patterns of AACNTs

Fig. 3 is Raman spectra of AACNTs. There are two obvious peaks centered at 1324.7 and 1593.2 cm^{-1}, namely D and G modes of CNTs, exhibited in the spectra. The D peak at 1324.7 cm^{-1} stems from a symmetry-lowering effect due to the defects of nanotube and amorphous structure. The G peak at 1593.2 cm^{-1} indicates the graphite crystallinity of this carbon material and it is generally used to identify well-ordered CNTs. The ratio of I_D to I_G is used to characterize the structure integrity of carbon materials. In general, the high value of I_D/I_G indicates that the sample has poor graphite crystallinity. The as-prepared AACNT samples have a relative high ratio of I_D/I_G (1.387) compared to the crystalline CNTs (0.045), showing that there exist large amounts of defects in the amorphous structures. The XRD patterns (see Fig. 4) of the comparison of AACNTs and the crystalline CNTs further proves the amorphous structure. The peak of the crystalline CNTs is sharp and far larger than that of AACNTs. The peak of AACNTs is more like a mild saddle compared with that of the crystalline CNTs.

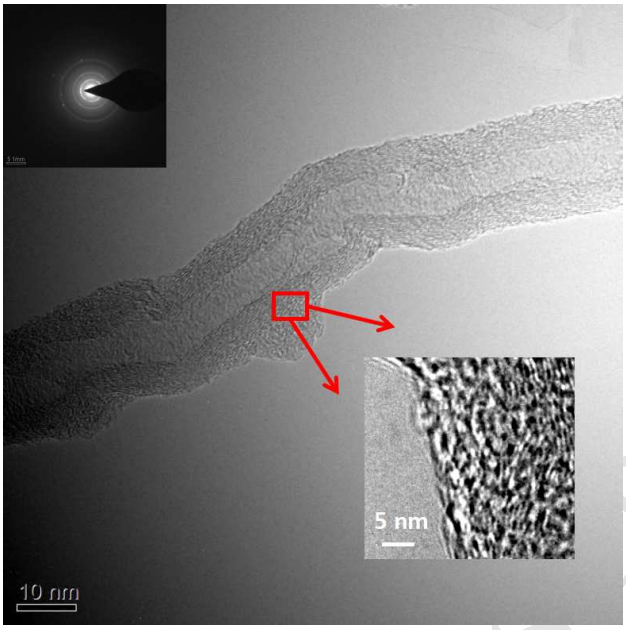

Fig. 5 TEM image of AACNTs. The diffraction rings is on the left-top. The high magnification of TEM is on the right-bottom.

Fig. 5 is TEM image of AACNTs. There exist small graphene sheets inside the as-grown CNT tube-walls and it can be seen from the high magnification picture on the right-bottom that carbon clusters are lined in random positions within long-distance range, indicating the amorphous structure has been formed. The diffraction rings of the SAED also prove the existence of amorphous structure.

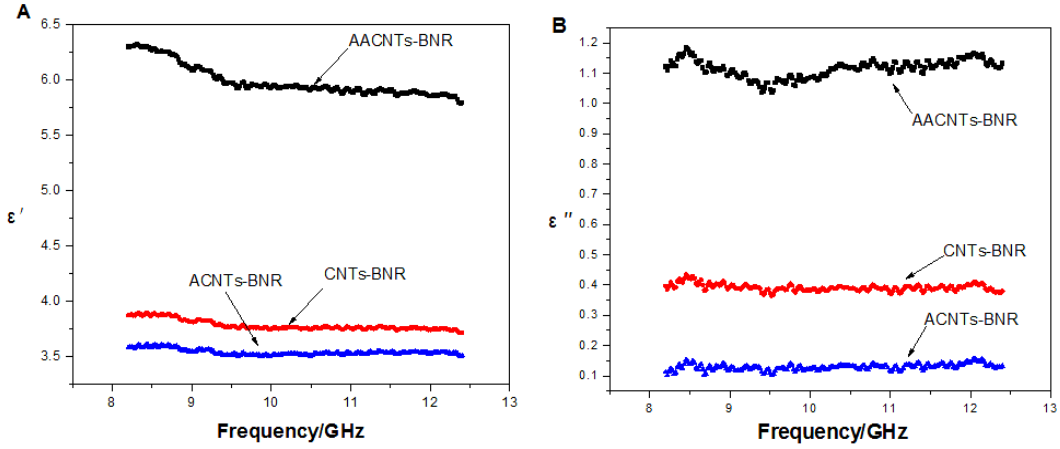

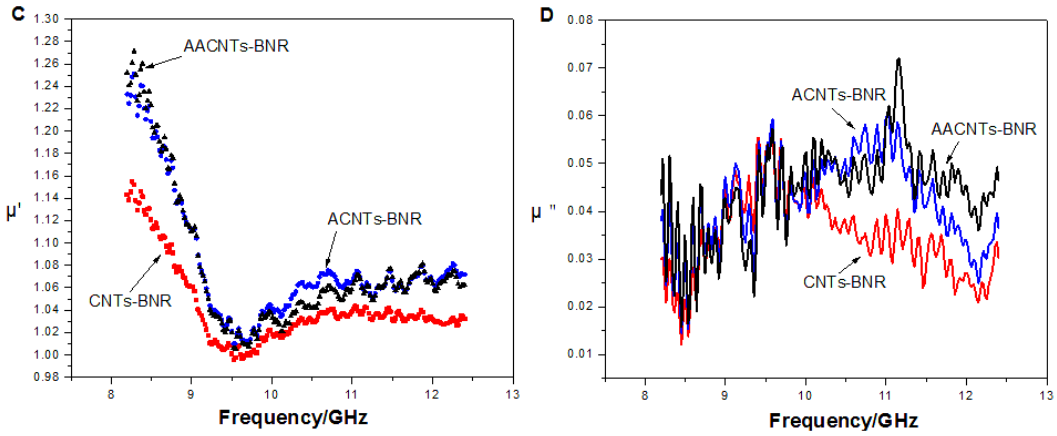

Fig. 6 Complex permittivity (ε', ε'') and permeability (μ', μ'') spectra of AACNTs-BNR composite *vs* frequency. (a, b) are the complex permittivity. (c, d) are the complex permeability

The complex permittivity (ε', ε'') and permeability (μ', μ'') spectra of AACNT/BNR composite *vs* frequency are shown in Fig. 6(a-d). The permittivity and permeability are used for characterization of dielectric constant and magnetic loss properties of the absorbing materials. In Fig. 6(a, b), the dielectric constant (ε') and dielectric loss (ε'') decrease slightly with frequency increasing, which is a normal behavior and is also observed by other researchers **[10]**. In Fig. 6(a, b), the dielectric constant (ε') and dielectric loss (ε'') of ACNTs-BNR are lower than that of CNTs-BNR, which can be explained as that the conductivity of ACNTs is not as good as CNTs due to the disordered structures inside the tube-walls. However, with the same amorphous structure as ACNTs, the ε' and ε'' of AACNT/BNRs is higher than both of ACNT/BNRs and CNT/BNRs. It can be assumed that the long linear pack structure of the array as well as Fe catalyst particles increase the conductivity, which makes AACNTs possess both the advantages of amorphous structure (the small graphite clusters inside the tube-wall can cause the scattering and increase the path length) and

crystal structure (good conductivity). AACNT/BNR composite has a better dielectric polarization and relaxation effects despite the poor conductivity of amorphous structure. When the conductive phase is distributed in the insulated matrix to form composite materials, the free charge gathered will exist in the interface between insulation and conductor due to the difference in the two phase conductive performance. The high tube density of the array structure may increase the probability for the tubes to overlap and twine each other for forming conductive network inside $BaFe_{12}O_{19}$ to improve the dielectric polarization properties. Besides, the similar orientation of the array may also benefit the dielectric polarization properties and the high length-diameter ratio of CNT arrays is also beneficial to the conductivity, and the dielectric loss. In Fig. 6(c, d), it is worth noting that a minimum value as well as a maximum value are observed for μ' and μ'', respectively, those obvious peaks for μ' and μ'' can be ascribed to a resonance phenomenon, which is also showed in Fig. 7b. The trend of the lines in Fig. 6(c, d) is similar, because carbon nanomaterials have poor magnetic loss and the several lines are all reveal the properties of $BaFe_{12}O_{19}$

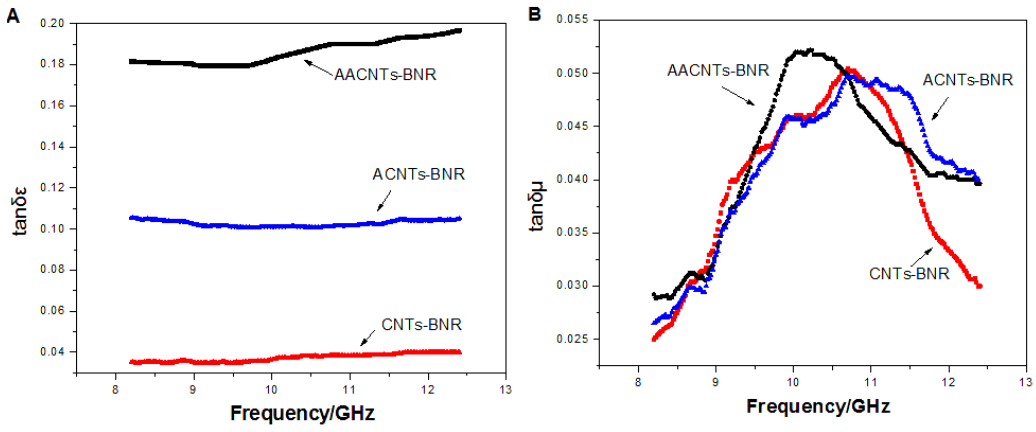

Fig. 7 Dielectric loss tangent ($\tan\delta_\varepsilon$) and magnetic loss tangent ($\tan\delta_\mu$) of AACNTs/BNR

composite *vs* frequency. (a) is the dielectric loss tangent ($\tan\delta_\varepsilon$) (b) is the magnetic loss tangent ($\tan\delta_\mu$)

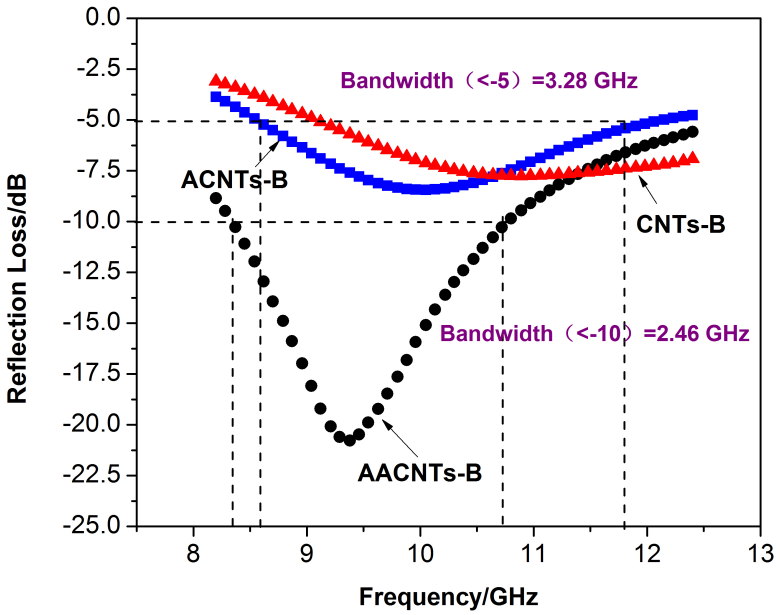

Fig. 8 Electromagnetic wave absorbing properties of AACNT/BNR composite

$$R(dB) = 20\log_{10}\left|\frac{Z_{in}-1}{Z_{in}+1}\right| \tag{1}$$

$$Z_{in} = \left(\frac{\mu_r}{\varepsilon_r}\right)^{\frac{1}{2}} \tanh\left[j\left(\frac{2\pi fd}{c}\right)(\mu_r\varepsilon_r)^{\frac{1}{2}}\right] \tag{2}$$

The surface reflectivity of an absorber was presented by a function including six parameters of ε', ε'', μ', μ'', f and d [23-25]. Thus, if the 5 parameters are known, the other parameters can be calculated. The values of reflectivity were calculated by using Eqs. (1) and (2) using the measured values of ε', ε'', μ', μ'', f and d (see Fig. 8). In the frequency range of 8-13 GHz, the maximum absorbing peak of AACNT/BNR composite is -21.5 dB at 9.3 GHz. The bandwidth of the reflectivity below -10 dB is 2.5 GHz. The maximum absorbing peak of ACNT/BNR composite is about -8.5 dB at

10.0 GHz, the bandwidth of the reflectivity below -5 dB is 3.3 GHz. In contrast, under the same matching thickness (d_m = 2.0 mm), the absorbing peak of CNT/BNRs becomes more flat and wide, the maximum absorbing peak of CNT/BNRs is about -7.5 dB at 10.7 GHz. Compared to the disordered ACNT samples, the AACNTs exhibits much larger reflection loss. It can also be proved through Fig. 7 (a) that the dielectric loss tangent ($\tan\delta_\varepsilon$) of AACNT/BNR sample is much higher than that of the other two samples. The electromagnetic wave absorbing mechanism of AACNT/BNR composite is depicted in Fig. 9. The excellent electromagnetic wave absorbing properties of the array structures may be explained by the follow two reasons. Firstly, the array structure with high density organized tubes formed an ordered conductive network inside $BaFe_{12}O_9$. The tubes possess excellent electrical conductivity and high aspect ratios. The conducting networks would interact and attenuate the electromagnetic radiation in the absorbers effectively. Secondly, the array structures with highly similar orientation tubes and the special structures of ACNTs with quantities of dihedral angles can consume the incident waves through multiple reflection and scattering inside the array structures. Compared with crystalline CNTs, the dihedral angles could be easily formed in the graphene sheet stacks within ACNT tube-walls, which cause multiple reflections of electromagnetic wave, prolonging the propagation path of electromagnetic waves in the absorbers **[10]**.The multiple reflections between the graphene sheet stacks in ACNTs explain why the electromagnetic wave absorbing performance is better than that of CNTs. The multiple reflections of microwave lead to the higher losses of electromagnetic energy.

Furthermore, the interaction of microwaves with dielectric materials intensified the molecular motions such as ionic conduction, dipolar polarization relaxation, etc., leading to energy dissipation in the form of heat through molecular friction and dielectric loss, and the highly conductive network would also consume the microwave as resistance heat.

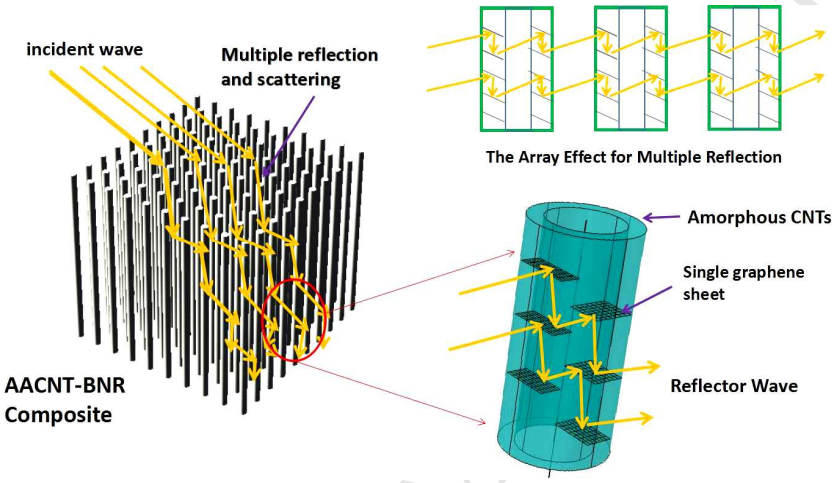

Fig. 9 Electromagnetic wave absorbing mechanism schematics of AACNT/BNR composite

4. **Conclusions**

AACNT/BNR composite was synthesized by floating catalyst CVD and ball-milling methods using AACNT arrays and $BaFe_{12}O_{19}$ nanorods as raw materials at 800 □. The average length of as-prepared ACNT arrays was about 24 μm and the average length of BNRs were about 50 nm. The maximum absorbing peak of AACNT/BNR composite is -21.5 dB at the frequency of 9.3 GHz. The frequency bandwidth of the reflectivity loss below -10 dB is about 2.5 GHz. AACNTs have both features of amorphous CNTs which have multiple-reflective path inside the tube-wall and crystalline CNTs which have high conductivity. It is found that the array structures as well as the amorphous morphology cause multiple reflections of

electromagnetic wave and prolongs the propagation path of electromagnetic waves in the absorbers, which leads to the consumption of incident waves. Besides, the array structures form an ordered conductive network inside the $BaFe_{12}O_9$ to interact and attenuate the electromagnetic radiation in the absorbers effectively.

Acknowledgments

This work was supported by the Specialized Research Fund for the Doctoral Program of Higher Education (20096102120016), Natural Science Foundation of China (5157222, 51672221), China Aeronautical Science Fund (2014ZF53074), the Key Science and Technology Program of Shaanxi Province, China (2013K09-03), and the "111" Project (B08040).

References

[1] S. Iijima, Helical microtubles of graphitic carbon, Nature 354 (1991) 56-58.

[2] S.J. Hwang, Y.S. Chuang, Enhanced hydrogen storage properties of MgH_2 co-catalyzed with zirconium oxide and single-walled carbon nanotubes, J. Alloys Compd. 664 (2016) 284-290.

[3] M.Y. Koo, G.W. Lee, S.B. Park, S.S. Kang, Y.S. Park, H.C. Shin, J.Y. Kim, D.H. Park, K.H. Ahn, S.J. Kang, W.S. Kim, Decoration of multi-walled carbon nanotubes with Fe_xNi_{1-x} alloys and their magnetic properties, J. Alloys Compd. 693 (2016) 1083-1089.

[4] T.K. Zhao, X.L. Ji, H.Z. Liu, P.Y. Yao, W.J. Liu, C.Y. Xiong, T.X. Li, C. Wang,

Growth of well-aligned carbon nanotubes with different shapes, Appl. Surf. Sci. 357 (2015) 2136-2140.

[5] H. Shao, X. Li, Effect of nanostructure and partial substitution on gas absorption and electrochemical properties in Mg_2Ni-based alloys, J. Alloys Compd. 667 (2016) 191-197.

[6] G. Dukovic, B.E. White, Z.Y. Zhou, F. Wang, S. Jockusch, M.L. Steigerwald, T.F. Heinz, R.A. Friesner, N.J. Turro, L.E. Brus, Reversible surface oxidation and efficient luminescence quenching in semiconductor single-wall carbon nanotubes, J. Am. Chem. Soc. 126 (2016) 15269-15276.

[7] Y. Wang, Z.X. Shi, J. Yin, Unzipped multiwalled carbon nanotubes for mechanical reinforcement of polymer composites, J. Phys. Chem. C 114 (2016) 19621-19628.

[8] X. Xu, S. Chen, C.H. Xiao, K. Xi, C.W. Guo, S.W. Guo, S.J. Ding, D.M. Yu, R.V. Kumar, Rational design of $NiCoO_2$@SnO_2 heterostructure attached on amorphous carbon nanotubes with improved lithium storage properties, ACS Appl. Mater. Inter. 8 (2016) 6004-6010.

[9] X. Xu, D.M. Yu, H. Zhou, L.S. Zhang, C.H. Xiao, C.W. Guo, S.W. Guo, S.J. Ding, MoS_2 nanosheets grown on amorphous carbon nanotubes for enhanced sodium storage, J. Mater. Chem. A 4 (2016) 4375-4379.

[10] T.K. Zhao, C.L. Hou, H.Y. Zhang, R.X. Zhu, S.F. She, J.G. Wang, T.H. Li, Z.F. Liu, B.Q. Wei, Electromagnetic wave absorbing properties of amorphous carbon nanotubes, Sci. Rep. 4 (2014) 5619-5619.

[11] Z. He, S.H. Qi, X.L. Zhong, H. Ma, P. Wang, H. Qiu, Preparation and microwave-absorbing properties of silver-coated strontium ferrite with polyaniline via in situ polymerization, J. Alloys Compd. 621 (2015) 194-200.

[12] X.Y. Yuan, L>F. Cheng, L.T. Zhang, Electromagnetic wave absorbing properties of SiC/SiO_2, composites with ordered inter-filled structure, J. Alloys Compd. 680 (2016) 604-611.

[13] T. B. Ghzaiel, W. Dhaoui, F. Schoenstein, P. Talbot, F. Mazaleyrat, Substitution effect of Me=Al, Bi, Cr and Mn to the microwave properties of polyaniline/$BaMeFe_{11}O_{19}$, for absorbing electromagnetic waves, J. Alloys Compd. 692 (2017) 774-786.

[14] Z. Mosleh, P. Kameli, A. Poorbaferani, M. Ranjbar, H. Salamati, Structural, magnetic and microwave absorption properties of Ce-doped barium hexaferrite, J. Magn. Magn. Mater. 397 (2016) 101-107.

[15] C.J. Wu, Z. Yu, Y. Yang, K. Sun, J.L. Nie, Y. Liu, X.N. Jiang, Z.W. Lan, Computational and experimental study on the cation distribution of La-Cu substituted barium hexaferrites, J. Alloys Compd. 664 (2016) 406-410.

[16] S.P. Pawar, M. Gandi, S. Bose, High performance electromagnetic wave absorbers derived from PC/SAN blends containing multiwall carbon nanotubes and Fe_3O_4 decorated onto graphene oxide sheets, RSC Adv. 6 (2016) 37633-37645.

[17] H. Mei, D.Y. Han, S.S. Xiao, T.M. Ji, J. Tang, L.F. Cheng, Improvement of the electromagnetic shielding properties of C/SiC composites by electrophoretic

deposition of carbon nanotube on carbon fibers, Carbon 109 (2016) 149-153.

[18] S.H. Lee, D.H. Kang, I.K. Oh, Multi layered graphene-carbon nanotube-iron oxide three-dimensional hetero structure for flexible electromagnetic interference shielding film, Carbon 111 (2017) 248-257.

[19] L.J. Yu, Y.F. Zhu, C. Qian, Q. Fu, Y.Z. Zhao, Y.Q. Fu, Nanostructured barium titanate/carbon nanotubes incorporated polyaniline as synergistic electromagnetic wave absorbers, J. Nanomater. 2016 (2016) 1-8.

[20] N. Shiri, A. Amirabadizadeh, A. Ghasemi, Influence of carbon nanotubes on structural, magnetic and electromagnetic characteristics of Mn, Mg, Ti, Zr substituted barium hexaferrite nanoparticles, J. Alloys Compd. 690 (2017) 759-764.

[21] M. Li, X.W. Yin, L.Q. Chen, M.K. Han, L.F. Cheng, L.T. Zhang, Dielectric and electromagnetic wave absorption properties of reduced graphene oxide/barium aluminosilicate glass-ceramic composites, Ceram. Int. 42 (2016) 7099-7106.

[22] T.K. Zhao, Y.N. Liu, J.W. Zhu, Temperature and catalyst effects on the production of amorphous carbon nanotubes by a modified arc discharge, Carbon 43 (2005) 2907-2912.

[23] N. Zhou, Q.D. An, W. Zheng, Z.Y. Xiao, S.R. Zhai, High-performance electromagnetic wave absorbing composites prepared by one-step transformation of Fe^{3+} mediated egg-box structure of seaweed, RSC Adv. 6 (2016) 98128-98140.

[24] B. Qu, C.L. Zhu, C.Y. Li, X.T. Zhang, Y.J. Chen, Coupling hollow Fe_3O_4-Fe nanoparticles with graphene sheets for high-performance electromagnetic wave

absorbing material, ACS Appl. Mater. Interfaces 8 (2016) 3730-3735.

[25] Y. Huang, X. Ding, S.P. Li, N. Zhang, J.G. Wang, Magnetic reduced graphene oxide nanocomposite as an effective electromagnetic wave absorber and its absorbing mechanism, Ceram. Int. 42 (2016) 17116-17122.

- The bandwidth of the AACNTs/BNR is about 2.5 GHz.
- Influences of the amorphous structure on wave absorbing performance.
- The length of as-prepared ACNT array was about 24 μm.